

## **❸ Variations of Northern Hemisphere Storm Track and Extratropical Cyclone Activity Associated with the Madden–Julian Oscillation**

YANJUAN GUO AND TOSHIAKI SHINODA

*Department of Physical and Environmental Sciences, Texas A&M University–Corpus Christi,  
Corpus Christi, Texas*

JIALIN LIN

*Department of Geography, Ohio State University, Columbus, Ohio*

EDMUND K. M. CHANG

*School of Marine and Atmospheric Sciences, Stony Brook University, State University of New York,  
Stony Brook, New York*

(Manuscript received 12 July 2016, in final form 28 February 2017)

### ABSTRACT

This study investigates the intraseasonal variations of the Northern Hemispheric storm track associated with the Madden–Julian oscillation (MJO) during the extended boreal winter (November–April) using 36 yr (1979–2014) of reanalysis data from ERA-Interim. Two methods have been used to diagnose storm-track variations. In the first method, the storm track is quantified by the temporal-filtered variance of 250-hPa meridional wind (vv250) or mean sea level pressure (pp). The intraseasonal anomalies of vv250 composited for eight MJO phases are characterized by a zonal band of strong positive (or negative) anomalies meandering from the Pacific all the way across North America and the Atlantic into northern Europe, with weaker anomalies of opposite sign at one or both flanks. The results based on pp are consistent with those based on vv250 except for larger zonal variations, which may be induced by surface topography. In the second method, an objective cyclone-tracking scheme has been used to track the extratropical cyclones that compose the storm track. The MJO-composite anomalies of the “accumulated” cyclone activity, a quantity that includes contributions from both the cyclone frequency and cyclone mean intensity, are very similar to those based on pp. Further analysis demonstrates that major contribution comes from variations in the cyclone frequency. Further analysis suggests that the intra-seasonal variations of the storm track can be primarily attributed to the variations of the mean flow that responds to the anomalous MJO convections in the tropics, with possible contribution also from the moisture variations.

### 1. Introduction

Storm tracks are midlatitude regions that are characterized by frequent passage of extratropical cyclones—storms. These storms are also referred to as baroclinic waves, transient eddies, or synoptic-scale disturbances in the literature, which we will also use in this study under proper context. In the climate community, the

activity of these storms is also called the storm track. Storm tracks play critical roles in both weather and climate. Extratropical cyclones are responsible for most of the severe and hazardous weather in the midlatitudes. They also transport a large amount of heat, momentum, and moisture and thus are important in maintaining the general circulation.

There are two basic methods to quantify the storm track. The first one identifies the extratropical cyclones, tracks their positions with time, and produces statistics for their distributions (e.g., Klein 1957; Hodies 1999; Hoskins and Hodges 2002), while the other one computes temporal bandpass-filtered eddy variance/covariance at a set of grid points with a retained frequency band

---

❸ Denotes content that is immediately available upon publication as open access.

---

Corresponding author e-mail: Yanjuan Guo, yanjuan.guo@tamucc.edu

highlighting the synoptic time scales (e.g., Blackmon 1976; Blackmon et al. 1977). Blackmon (1976) found that the geographical locations of bandpass-filtered (2–6 days) eddy variance of 500-hPa geopotential height correspond closely to the regions with frequent occurrence of extratropical cyclones and thus used the term storm tracks to describe the maxima of these eddy statistics. It should be noted that eddy statistics do not differentiate between cyclones and anticyclones and thus include contributions from both. However, anticyclones (high pressure systems) are usually slow-moving and have pressure anomalies much weaker compared to cyclones (e.g., Hoskins and Hodges 2002). Climatological distribution also indicates that they are located farther equatorward, suggesting that they mainly reflect the variations of the subtropical high (Hoskins and Hodges 2002). Therefore, the eddy statistics are likely dominated by the contributions from the cyclones, and we will not discuss the anticyclones in this study.

There are both advantages and disadvantages in using the **cyclone tracking** and **eddy statistics methods**. The cyclone-tracking, or Lagrangian, method is straightforward and easily related to the daily weather. However, the tracked cyclones are sparsely distributed in time and space with large spread in intensity, making it difficult to identify general relationships between cyclones and the large-scale meteorological conditions. On the other hand, Eulerian eddy statistics such as the eddy momentum, heat, and moisture fluxes are important terms in the governing equations for momentum, heat, or moisture. Thus, it is convenient to diagnose the interaction between eddies and mean state by examining these quantities. However, eddy statistics do not provide specific information regarding the cyclones, such as the intensity or frequency of occurrence. **Therefore, it is necessary to examine results based on both methods such that complementary information can be obtained.**

Because of the importance of storm track in both weather and climate, it is important to investigate the characteristics of the storm tracks, especially their variability, which often causes significant regional weather and climate variations. In this study, we will examine the intraseasonal variability of storm track associated with the Madden–Julian oscillation (MJO).

The MJO is the dominant mode of intraseasonal (30–90 day) variability in the tropics, characterized by slow ( $\sim 5 \text{ m s}^{-1}$ ) and planetary-scale eastward propagation of convection and circulation anomalies (Madden and Julian 1971, 1972; Zhang 2005). Owing to the strong heating anomalies involved, the MJO can produce strong response not only in the tropics but also in the extratropics.

The extratropical response to tropical diabatic heating anomalies has long been noticed as the teleconnection patterns (Horel and Wallace 1981; Wallace and Gutzler 1981) and interpreted in terms of Rossby wave dispersion by Hoskins and Karoly (1981). Since then a number of studies have investigated the extratropical response to the tropical convection anomalies on the intraseasonal time scale, mostly focusing on the Northern Hemisphere (NH) large-scale circulation (Liebmann and Hartmann 1984; Weickmann et al. 1985; Lau and Phillips 1986; Knutson and Weickmann 1987; Ferranti et al. 1990; Hsu 1996; Matthews and Kiladis 1999; Matthews and Meredith 2004; Lin et al. 2009, 2010; Straus et al. 2015; Henderson et al. 2016; among many others).

Previous studies on the extratropical response to the MJO have mostly focused on large-scale circulation anomalies. It is only very recently that a number of studies started to examine the MJO influence on the midlatitude storm tracks and extratropical cyclones (Deng and Jiang 2011, hereafter DJ11; Lee and Lim 2012, hereafter LL12; Grise et al. 2013, hereafter Grise13; Takahashi and Shirooka 2014). Prior to these studies, Matthews and Kiladis (1999) analyzed the interaction between the midlatitude high-frequency transients and the MJO. However, the “high frequency” in this study corresponds to the 6–25-day variability instead of the typical time scale of the midlatitude storms (about 2–6 days). DJ11 performed a multivariate empirical orthogonal function (MEOF) analysis of the intraseasonal filtered tropical outgoing longwave radiation (OLR) and the North Pacific storm track quantified by vertically averaged synoptic eddy kinetic energy (SEKE) and derived the coupling pattern between the MJO convection and the Pacific storm track by compositing strong coupling events identified by the principal components (PCs) of the MEOF. They found that the North Pacific winter storm-track response is characterized by an amplitude-varying dipole propagating northeastward as the center of the anomalous tropical convection moves eastward across the eastern Indian Ocean and the western-central Pacific. Takahashi and Shirooka (2014) further extended the work by DJ11 by separating the MJO events according to different El Niño–Southern Oscillation (ENSO) conditions. LL12 used the envelope of the 2.5–6-day bandpass-filtered variance of 250-hPa geopotential height to represent the storm activity and composited it through the MJO RMM index developed by Wheeler and Hendon (2004; WH; see section 2c for more details) to investigate the impacts of the MJO convection on the zonal location and intensity of the North Pacific storm activity. These three studies are all based on the Eulerian eddy statistics method.

In this study, we will investigate the influence of the MJO on the storm track using both Lagrangian cyclone-tracking and Eulerian eddy statistics methods, and results will be compared in the same context. A recent study by [Grise13](#) discussed the variations of the extratropical cyclones over North America associated with four climate phenomena: the NAO, ENSO, the PNA, and the MJO using the cyclone-tracking method. While they detected some signals of storm-track activity associated with the MJO, it is difficult to directly compare their results with those based on Eulerian statistics in previous studies such as [DJ11](#) and [LL12](#) because of the differences regarding the region focused on, the variables analyzed, and the compositing method. For example, [Grise13](#) focused on North America, while [DJ11](#) and [LL12](#) focused on the North Pacific; [DJ11](#) used the vertically integrated SEKE, and [LL12](#) used the envelope of eddy variance of meridional wind to measure the storm-track activity, while [Grise13](#) tracked the local maxima of the positive vorticity at 850 hPa; [DJ11](#) identified coupling events between the MJO and the storm track by PCs of MEOF, while [LL12](#) and [Grise13](#) used the WH MJO RMM index. In this study, we will examine the MJO's influence on the storm track for the entire NH instead of a particular sector. To make as fair as possible comparison, we will use mean sea level pressure (MSLP) in both the eddy statistics and cyclone-tracking methods and composite the MJO events using the MJO RMM index. The examination of the results based on the cyclone-tracking methods as well as the comparison to those based on eddy statistics will provide more insights that have not been obtained regarding the storm-track variations associated with the MJO.

The rest of this paper is organized as follows. [Section 2](#) describes the data and methodology used in this paper. [Sections 3](#) and [4](#) then present the intraseasonal variations of the storm track and extratropical cyclone activity associated with the MJO from eddy statistics and cyclone-tracking perspectives, respectively. In [section 5](#), we will examine two physical factors through which the MJO may modulate the storm track. Finally, the conclusions and discussion are presented in [section 6](#).

## 2. Data and methodology

### a. Data

The primary dataset used in this study is the ECMWF interim reanalysis (ERA-Interim; [Dee et al. 2011](#)). Atmospheric variables including meridional and zonal winds, specific humidity, MSLP, geopotential height at several significant pressure levels, and the total column water vapor (TCWV) are used. All variables were first interpolated onto the same horizontal resolution of  $2.5^\circ$  by

$2.5^\circ$ . Daily averaged values are used except for conducting the automated cyclone tracking. In the cyclone-tracking procedure, 6-hourly data are used since high-temporal-resolution data are required for forming reasonably continuous tracks. The time period examined is 36 yr from January 1979 to December 2014.

In addition to the ERA-Interim data, precipitation data from the Tropical Rainfall Measuring Mission (TRMM) 3B42 version 7 ([Huffman et al. 2007](#)) are used as a proxy of the tropical deep convection to detect the MJO signal. They were interpolated onto the same temporal and horizontal resolutions as the reanalysis. The temporal coverage of the precipitation data is from January 1998 to December 2012.

This study focuses on the Northern Hemisphere and the extended boreal winter season (November to April) for the following two reasons: 1) the storm track is much stronger in winter than that in summer owing to stronger meridional temperature gradient, and 2) boreal winter is also the season when tropical convection is located in the near-equatorial region and the intraseasonal variability exhibits coherent eastward propagation. In boreal summer, the strongest tropical convection shifts northward and the intraseasonal variability often displays northward propagation in addition to the eastward propagation owing to its interaction with the Asian summer monsoon (e.g., [Waliser 2006](#)).

### b. Storm track

#### 1) CYCLONE TRACKING: A LAGRANGIAN PERSPECTIVE

The cyclone-tracking method dates back to the late nineteenth century when the cyclone tracks were manually identified on the daily synoptic charts (e.g., [Klein 1957](#)). Because of the substantial effort required for the manual tracking, this method had not been extensively used until recently when automatic objective algorithms were developed (e.g., [Bell and Bosart 1989](#); [Murray and Simmonds 1991](#); [Hodges 1999](#); among others). In this study, we will employ the objective tracking tool developed by [Hodges \(1994, 1995, 1999\)](#).

We follow the tracking procedures described by [Hodges \(1999\)](#) and [Hoskins and Hodges \(2002\)](#). In this study, the meteorological variable used is MSLP, in which surface cyclones will be tracked. Other variables, such as 850-hPa relative vorticity, 500-hPa geopotential height, 300-hPa potential vorticity, have also been used in different studies. Each of these variables has its own advantages and disadvantages, but examination of a great variety of variables reveals generally similar patterns ([Hoskins and Hodges 2002](#)). We will present results based on MSLP only in this study. Details of the tracking procedure are discussed below.

First, a spatial filtering by which only waves with total wavenumber equal to or greater than 5 are retained is applied to the 6-hourly MSLP data to remove the large-scale, low-frequency background flow (Hoskins and Hedges 2002). Local negative MSLP minima are then identified as the cyclone centers at each time step. Finally, these pressure minima are linked together across time steps to form cyclone tracks. The sets of optimized tracks are obtained by minimizing a cost function with constraints concerning the track smoothness and the maximum displacement of cyclones among consecutive time steps. Further details of the method are found in Hedges (1999). The outputs from the tracking algorithm include the longitude and latitude of the cyclone center, as well as the center intensity (the absolute value of the pressure anomaly) for each track at each time step. Note that cyclone intensity here refers to the pressure anomaly from a large-scale background flow, instead of the absolute minimum pressure at the cyclone center. Many recent studies (e.g., Lim and Simmonds 2002; Donohoe and Battisti 2009; Chang 2014) have suggested that it may be advantageous to use pressure perturbation rather than the absolute minimum pressure value to indicate cyclone intensity since the latter is strongly influenced by changes in the large-scale low-frequency background pressure field. Following Hoskins and Hedges (2002), we only use tracks with a minimum lifetime of 2 days and a minimum track length of 1000 km.

From these tracks, a daily,  $2.5^\circ$  by  $2.5^\circ$  gridded cyclone dataset from 1979–2014 was created by accounting all the cyclones within 500-km distance of a grid point. This is equivalent to assume that a cyclone has a radius of influence of 500 km, which has been widely used in previous studies (e.g., Sinclair 1997; Grise13). The center intensity is recorded. Since the tracking output is four times per day, there are cases when more than one cyclone is present in a grid box within one day. In such cases, the averaged intensity is used. It should be noted that here we assume the radius of influence of a cyclone is constant no matter which stage it is in and how strong it is, which is apparently not accurate enough. More sophisticated ways such as adding intensity-related weighting to the radius of influence or determining the radius by the closed isobar contour of a certain value could be applied but are beyond the scope of this study. Nevertheless, we performed sensitivity tests by changing the radius of influence to be 600 or 400 km, and results showed that our conclusions are not sensitive to the choice of the value of the radius of influence within this range.

## 2) EDDY VARIANCE-COVARIANCE: AN EULERIAN PERSPECTIVE

The second approach to diagnose the storm track is to use the bandpass-filtered eddy variance–covariance.

Since Blackmon (1976) first introduced the bandpass-filtered variance of 500-hPa geopotential height, many other eddy variance–covariance quantities have also been used to indicate storm tracks. In this study, we use the 24-h-difference-filtered variance introduced by Wallace et al. (1988). The 24-h difference filtering has half power points at periods of 1.2 and 6 days and thus is similar to the bandpass filtering for the synoptic time scale. For the case of meridional velocity  $v$ , the storm track is expressed as follows:

$$vv = \overline{[v(t + 24\text{h}) - v(t)]^2}, \quad (1)$$

in which  $v(t + 24\text{h}) - v(t)$  is the 24-h differenced  $v$  anomaly, which is calculated at each time step and each grid point. Then,  $vv$  is computed by averaging the squared  $v$  anomaly over a certain time period. Note that the averaging time period does not have to be continuous. For example, the MJO composite  $vv$  that we will discuss later is the average squared  $v$  anomaly for the days of a certain MJO phase.

### c. Madden–Julian oscillation index

In this study, we use the all-season real-time multivariate MJO (RMM) index developed by Wheeler and Hendon (2004) to composite the MJO cycle. The RMM index consists of a pair of indices (RMM1 and RMM2), which are the first two leading normalized principal components of the combined EOF analysis of equatorially averaged OLR and 850- and 200-hPa zonal winds. The evolution of the MJO is described as an eight-phase cycle by combining both the sign and magnitude of the RMM1 and RMM2 indices and is characterized by the eastward propagation of tropical convection as well as coherent circulation changes from the Indian Ocean to the Western Hemisphere and Africa. Given the RMM index, the MJO phase and amplitude of any particular day can be determined. Thus, the MJO composite of each field can be obtained by averaging the field through eight MJO phases based on the RMM index. In this study, only “strong” MJO days (defined as follows:  $\text{RMM1}^2 + \text{RMM2}^2 \geq 1$ ) are used.

Note that other MJO indices based on OLR only (Kiladis et al. 2014) have also been examined, and the results obtained are very similar to those based on the RMM index and thus are not shown here.

## 3. MJO influence on storm track based on eddy variance approach

In this section, the variations of storm track associated with the MJO will be examined by compositing the

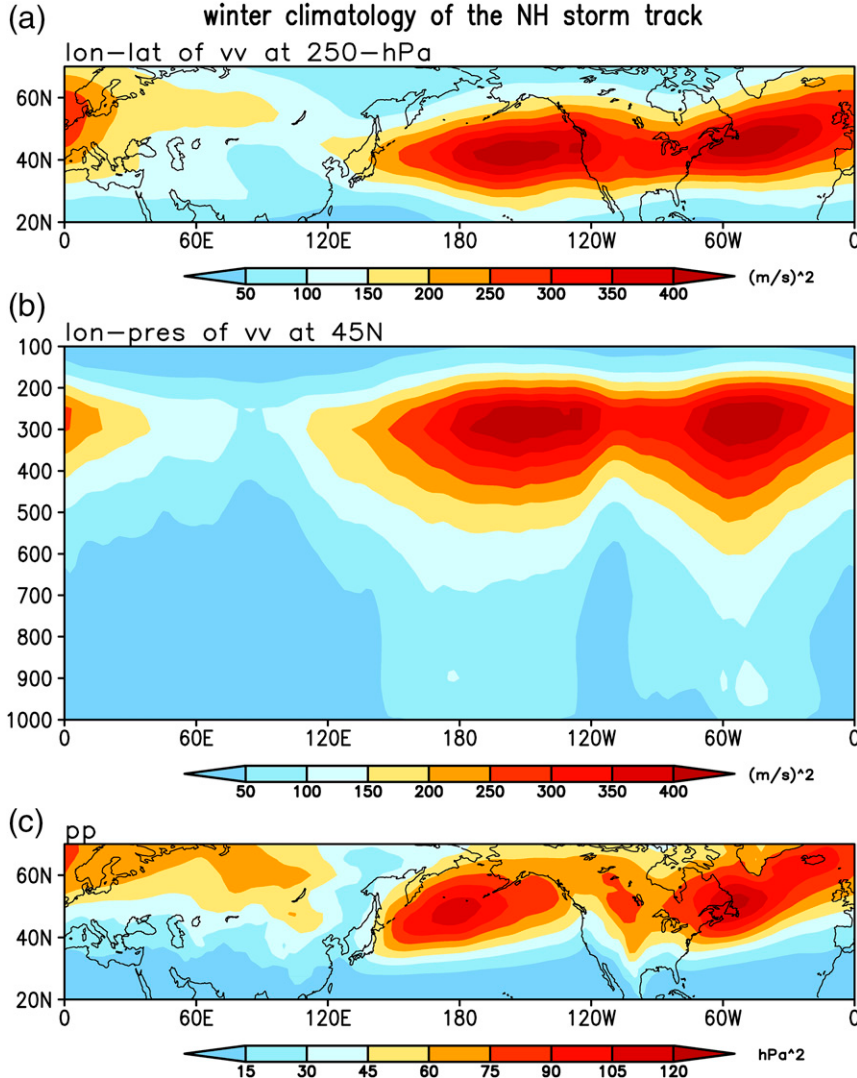


FIG. 1. Climatology of Northern Hemisphere storm tracks during 1979–2014 extended boreal winters (November–April) based on ERA-interim data. (a) Longitude–latitude vv plane at 250 hPa and (b) longitude–pressure cross section at 45°N of the 24-h-differenced variance of meridional wind (vv;  $\text{m}^2 \text{s}^{-2}$ ); (c) longitude–latitude plane of the 24-h-differenced variance of the mean sea level pressure (pp;  $\text{hPa}^2$ ).

storm-track anomalies with respect to different MJO phases. Results based on the eddy variance method will be first shown. Eddy variance of meridional wind is probably the most widely used measure of storm track since it represents the dominant part of the eddy kinetic energy, so much of our results will be based on this quantity. In addition, eddy variance of MSLP is also examined in order to provide direct comparison to the results based on the cyclone-tracking method, in which the MSLP field is used. Before examining the MJO-related anomalies, we will first examine the winter climatology of the NH storm track. While this has been discussed in previous studies, this provides important

information that will be useful when we examine the MJO composites later.

#### a. Climatology

The winter climatology of the NH storm track averaged over 36-yr (1979–2014) boreal winter seasons (November–April) is shown in Fig. 1. The three-dimensional structure of the NH storm tracks can be perceived by combining information from both the longitude–latitude plane at 250 hPa (Fig. 1a) and the longitude–pressure cross section along 45°N (Fig. 1b) of vv (i.e., 24-h-differenced variance of the meridional wind). From Fig. 1a, it is seen that vv at 250 hPa vv250 in

the NH cool season is most pronounced in the mid-latitudes and extends zonally from the western North Pacific, across North America and the North Atlantic, and into northern Europe, with two peaks over the central to eastern North Pacific and North Atlantic, which are the well-known Pacific and Atlantic storm tracks, respectively (Fig. 1a). The Pacific storm track is overall zonal and centered at around 45°N, while the Atlantic storm track is several degrees poleward of the Pacific one and shows noticeable southwest–northeast tilting. The longitude–pressure cross section along 45°N (Fig. 1b) indicates that the storm track based on vv peaks at the level of about 250 hPa, which corresponds to the level of the midlatitude jet core, as well as the approximate tropopause height. This is dynamically consistent since the main energy source of the baroclinic waves forming the storm track lies in the conversion of the mean available potential energy from the mean flow.

The storm track based on mean sea level pressure (pp; i.e., 24-h-differenced MSLP variance) (Fig. 1c) is very similar to that based on vv250 (Fig. 1a) with the North Pacific and North Atlantic storm tracks being pronounced. However, a few differences between Figs. 1c and 1a can be seen. First, the storm track based on pp is less zonally continuous from the Pacific to northern Europe, with an apparent break over the Rockies, while a secondary maximum over central North America is probably due to lee cyclones to the east of the Rockies. Second, the maxima of the Pacific and Atlantic storm tracks are both shifted toward the western part of the oceans; the Pacific storm track shows noticeable southwest–northeast tilt that is not evident in vv250, while the southwest–northeast tilt in the Atlantic storm track becomes more pronounced compared to that in vv250. These are probably due to the influence of the western boundary ocean currents (WBCs), such as the Kuroshio and Kuroshio Extension (e.g., Taguchi et al. 2009; Joyce et al. 2009; Nakamura et al. 2012; O'Reilly and Czaja 2015) and the Gulf Stream (e.g., Businger et al. 2005). It is speculated that the WBCs influence extratropical cyclones through low-level baroclinicity and/or diabatic heating associated with sensible and latent air-sea heat fluxes (Hoskins and Valdes 1990; Nakamura et al. 2008). Booth et al. (2010) also suggested the warm ocean current tends to shift the surface storm track to the south of the mid- to upper-tropospheric storm track owing to the reduction in near-surface static stability over the warm side of the current. The topographic influences seem to be more visible in the surface pressure than in the upper-level wind field. Furthermore, the entire NH storm tracks are a few degrees farther north in pp than those in vv250, which is probably due to the impact of the Coriolis parameter. The relationship

between  $v$  and pressure is quasigeostrophic; because of the smaller Coriolis parameter in low latitudes, the variances of  $p$  are displaced poleward compared to those of  $v$  (Trenberth 1991). As shown later, these differences are also inherited by the MJO composites. Nevertheless, the main characteristics of the NH storm tracks in boreal winter are highly consistent based on either the surface pressure or upper-level wind.

### b. MJO composite of storm-track anomalies

The MJO composites of vv250 during 1979–2014 boreal winters are displayed in Fig. 2. The procedure to form the composite is as follows. First, the 24-h-differenced anomaly of meridional wind is calculated for each calendar day at each grid point and squared. Then the climatological mean (1979–2014) of the squared anomaly is removed for each calendar day. Then, a 20–100-day bandpass filter is applied to the time series of the squared anomalies to isolate the intraseasonal variability. Finally, the intraseasonal-filtered anomalies are composited into the eight MJO phases using the RMM index for strong MJO days ( $RMM1^2 + RMM2^2 \geq 1$ ) during boreal winter. The number of total MJO days used for the composite for each phase is indicated at the upper-left corner of each panel. In Fig. 2, the composite anomalies displayed at nearly all the grid points are statistically significant at a 99% confidence level based on a two-tailed Student's  $t$  test; thus no significance contours are shown. (The same is true for Figs. 3, 8, 9, and 10.) Note that the degrees of freedom are smaller than the number of strong MJO days used for the MJO composite owing to possible autocorrelation in the time series of vv250 or pp anomalies (Leith 1973). The reduction of the degrees of freedom has been considered throughout this paper when performing the significance test.

The MJO-related vv250 anomalies are most pronounced over the North Pacific but also extend across North America and the North Atlantic into Europe, with only weak anomalies over most of the Eurasian continent (Fig. 2). The overall pattern is characterized by an elongated band of strong positive (or negative) anomalies over 35°–55°N meandering from the Pacific to the Atlantic with weaker anomalies of opposite sign at one or both flanks. Specifically, during MJO phase 1, weak positive anomalies extend eastward from Eurasia across the Pacific. These positive anomalies can be seen propagating eastward and strengthening, becoming strongest by phase 3. At that time a band of strong positive anomaly extends across the entire midlatitude Pacific, with weaker anomalies extending across the southern part of the United States into the Atlantic, with the signal reaching Europe by phases 4 and 5. Subsequently, these positive anomalies continue to shift

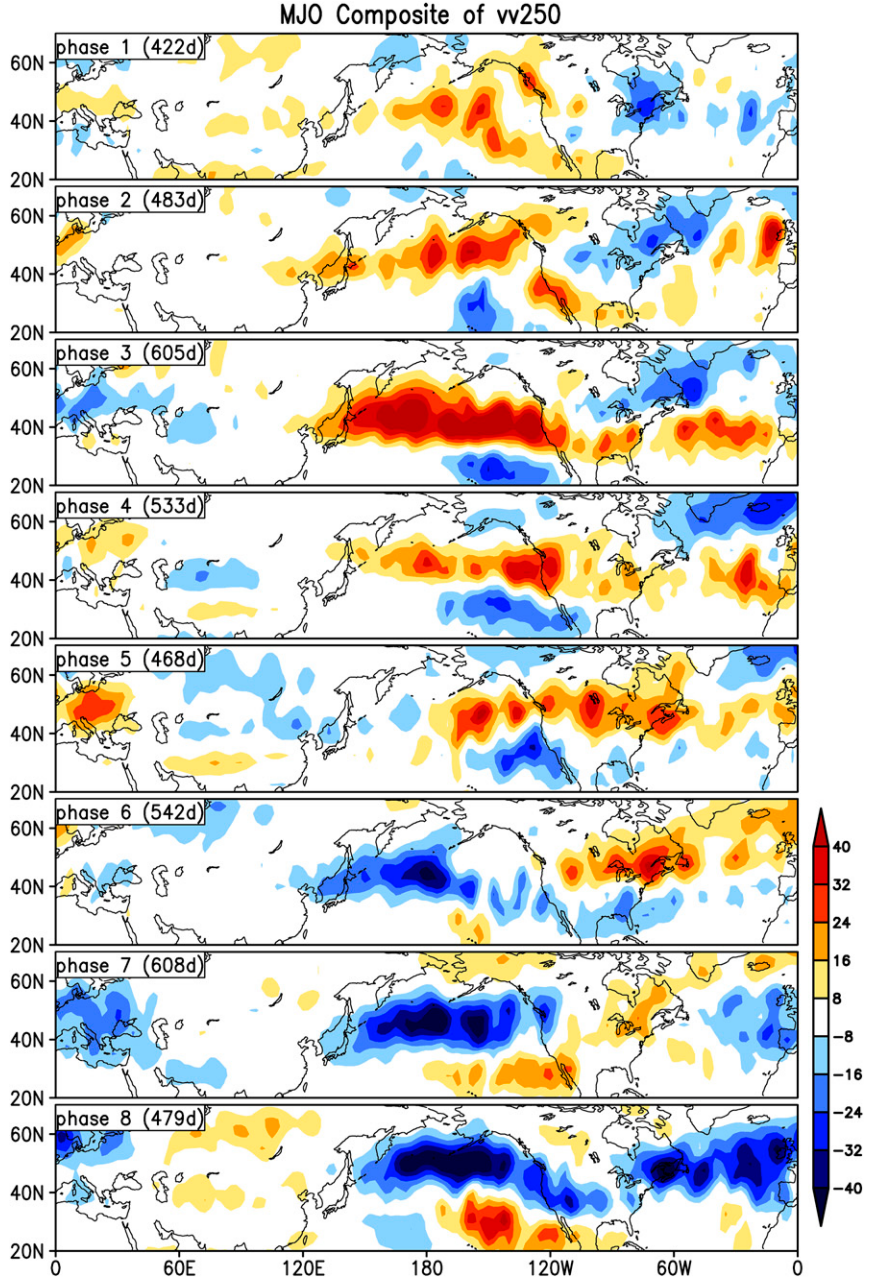


FIG. 2. Eight-phase MJO composites of the intraseasonal (20–100 day) filtered anomalies of the storm track quantified by the 24-h-difference variance of 250-hPa meridional wind ( $\text{m}^2 \text{s}^{-2}$ ). Only strong MJO days ( $\text{RMM1}^2 + \text{RMM2}^2 \geq 1$ ) during 1979–2014 winter seasons (November–April) are used for the composite whose number for each phase is indicated at the upper-left corner of each panel. Almost all the points within the shaded areas are significant at a 99% confidence level based on a two-tailed Student's *t* test, and thus no significance level is shown.

eastward and weaken, nearly disappearing by phase 8. Meanwhile, half a cycle later, similar but opposite-signed anomalies start developing over Eurasia and western Pacific during phase 5, moving eastward and strengthening, until strong negative anomalies extend

all the way from the Pacific across the southern United States and North Atlantic into northern Europe by phase 8. To the south of these main anomalies, we can also see anomalies of the opposite sign developing over the eastern Pacific.

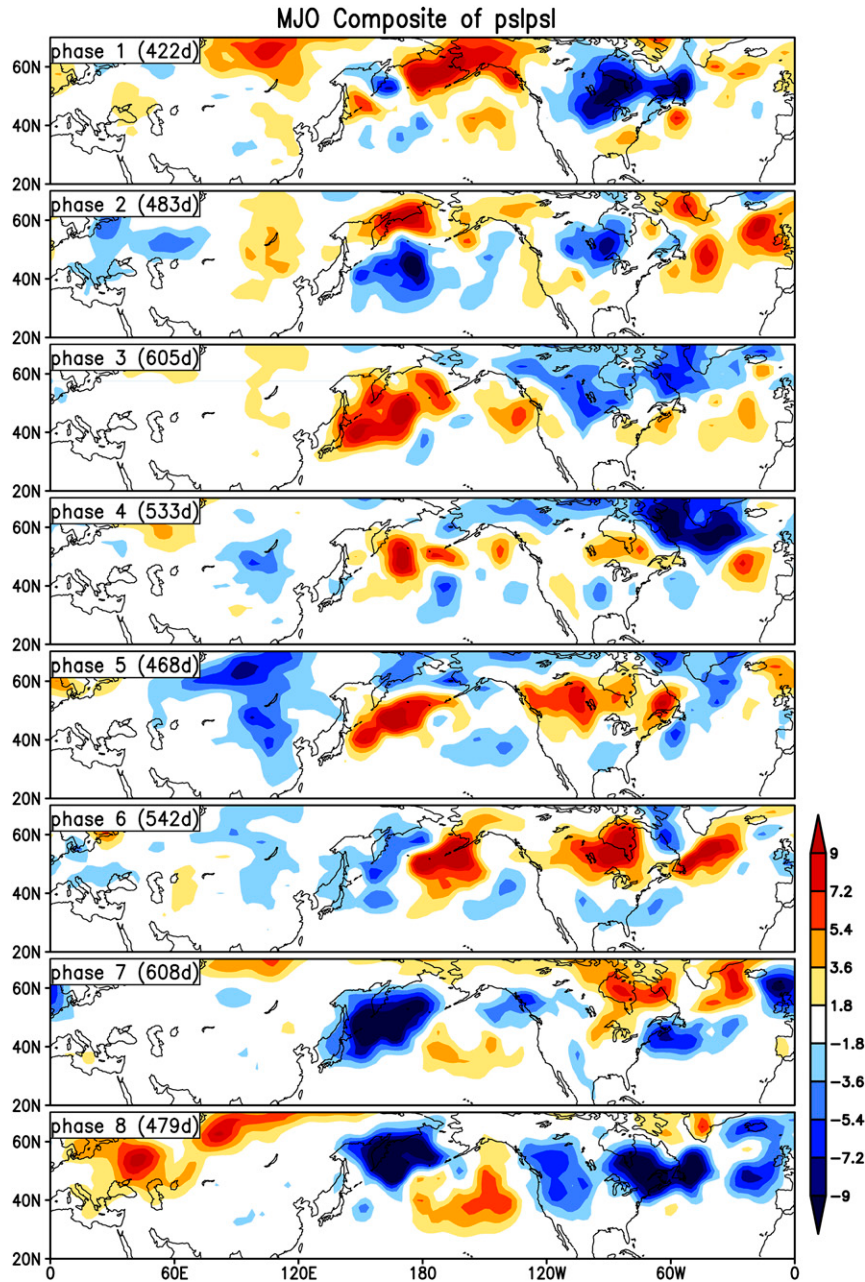


FIG. 3. As in Fig. 2, but for mean sea level pressure ( $\text{hPa}^2$ ).

Throughout the MJO cycle, the storm-track anomalies move eastward and slightly northward along with the eastward propagation of the MJO convection anomalies. (Note that the locations of the anomalous

MJO convection centers in each MJO phase are indicated by red contours in Figs. 8 and 9.) During MJO phases 1–4 when enhanced MJO convection propagates from the Indian Ocean to the Maritime Continent, the Pacific storm track is mainly intensified and becomes narrower, while the Atlantic storm track mainly shows

equatorward displacement. These characteristics are overall opposite for MJO phases 6–8 when suppressed MJO convection moves from the Indian Ocean to Maritime Continent.

Figure 3 further shows the storm-track anomalies associated with MJO based on  $\text{pp}$ . The anomalous patterns are largely consistent with those based on  $\text{vv250}$  (Fig. 2), except for some differences that can be traced back to differences in the climatology. First of all, the storm-track anomalies are not as zonally continuous as

those in Fig. 2. Stronger anomalies are found in the western oceans, especially over the Kuroshio Extension area, than those in the eastern oceans; very little variation is present over the Rocky Mountains, but anomalies are pronounced downstream of the Rockies. Also, the anomalies in the western Pacific exhibit strong southwest-to-northeast tilt, which is not found in Fig. 2. Again, these differences are probably due to the stronger influence of the ocean and land surface topography, such as the Kuroshio Extension and Rocky Mountains, on the storm track quantified by the surface pressure than that by the upper-level wind as we have seen in the climatology (Figs. 1a,c). Despite these differences, the overall distributions of storm-track anomalies based on vv250 and pp are quite similar, with positive anomalies extending from the western Pacific across North America into the Atlantic during phase 3 and the same for negative anomalies during phases 7 and 8.

The results suggest that the magnitude of the intra-seasonal storm-track anomalies associated with the MJO is about 1/10 of the magnitude of the climatology:  $40 \text{ versus } 400 \text{ m}^2 \text{ s}^{-2}$  for vv250 (Fig. 2 vs Fig. 1a) and  $10 \text{ versus } 100 \text{ hPa}^2$  for pp (Fig. 3 and Fig. 1c).

#### 4. MJO cycle of storm track based on cyclone-tracking approach

In this section, results based on the cyclone-tracking method will be presented and compared with the eddy variance method. Three parameters are used to describe the cyclone statistics at each grid point: 1) cyclone frequency, which is the number of cyclones divided by the number of days during which they are counted; 2) cyclone mean intensity, which is the averaged pressure anomaly of cyclone center for these cyclones; and 3) the “accumulated” cyclone activity, which is simply the product of cyclone frequency and cyclone mean intensity. It represents the accumulated pressure anomaly for all the cyclones during the time period considered, thus taking into account contributions from both the cyclone occurrence and cyclone strength.

##### a. Climatology

The winter climatology of the cyclone statistics based on the cyclones tracked during the boreal winter season (November–April) is shown in Fig. 4. The geographical distribution of the NH storm tracks is well captured by all three parameters, with the strongest cyclone activity being over the North Pacific and North Atlantic. The overall patterns are very similar to those based on the eddy variance of MSLP (Fig. 1c). Nevertheless, the cyclone frequency exhibits larger spatial variations within the storm tracks, while the mean intensity map indicates

that over the North Pacific and Atlantic Oceans the storms have generally comparable magnitudes. It is also of interest to note that the occurrence of cyclones are as frequent over North America from the eastern side of the Rockies to the East Coast as over the Pacific and Atlantic Oceans, but the intensity of these cyclones are much weaker compared to those over oceans. As a result, the accumulated cyclone activity exhibits a secondary storm track over this region, which is consistent with what is shown in the eddy variance of MSLP (Fig. 1c). Such differences between the cyclone frequency and mean intensity cannot be inferred from the eddy variance, which is a single quantity related to both frequency and intensity.

Figure 4 indicates that over the storm-track regions extratropical cyclones pass within 500 km of a certain point about once a week (Fig. 4a), and on average the pressure depression at the cyclone centers is about 20 hPa (Fig. 4b).

##### b. MJO composite of cyclone statistics

The cyclones during 1979–2014 boreal winters are further composited throughout the MJO cycle to show the MJO’s influence on the storm track, and the results are compared with those based on pp. Again, only strong MJO days ( $\text{RMM1}^2 + \text{RMM2}^2 \geq 1$ ) are used. The composite cyclone frequency, mean intensity, and accumulated activity are first computed for each MJO phase, and then the anomalous patterns relative to the winter climatology are shown by subtracting the climatology from the composite for each phase. Note that the compositing procedure is somewhat different from what we have done for the eddy variance quantities in which the annual cycle of the time series is first removed and an intraseasonal filtering is applied to obtain the anomalies. The reason is that cyclones occur only on about 10% of the days of the time series, which makes the daily climatology very noisy, and the time filtering is impractical. Thus we examine the mean anomalies of each phase relative to the climatology for the entire period.

Figures 5–7 show that results based on the tracking method are overall noisy, consistent with the results of Grise13. Despite the relatively high noise level, the cyclone frequency does exhibit systematic variations in the form of large areas of negative or positive anomalies throughout the MJO cycle (Fig. 5), and these anomalous patterns show considerable similarities to the MJO composites of pp anomalies shown in Fig. 3 (e.g., the overall increased cyclone occurrence over the Bering Sea and Alaska in phase 1, the dipole with increased cyclones in the north and reduced cyclones in the south of the North Pacific in phase 2, and overall decreased cyclone occurrences off Japan during phases 5–8).

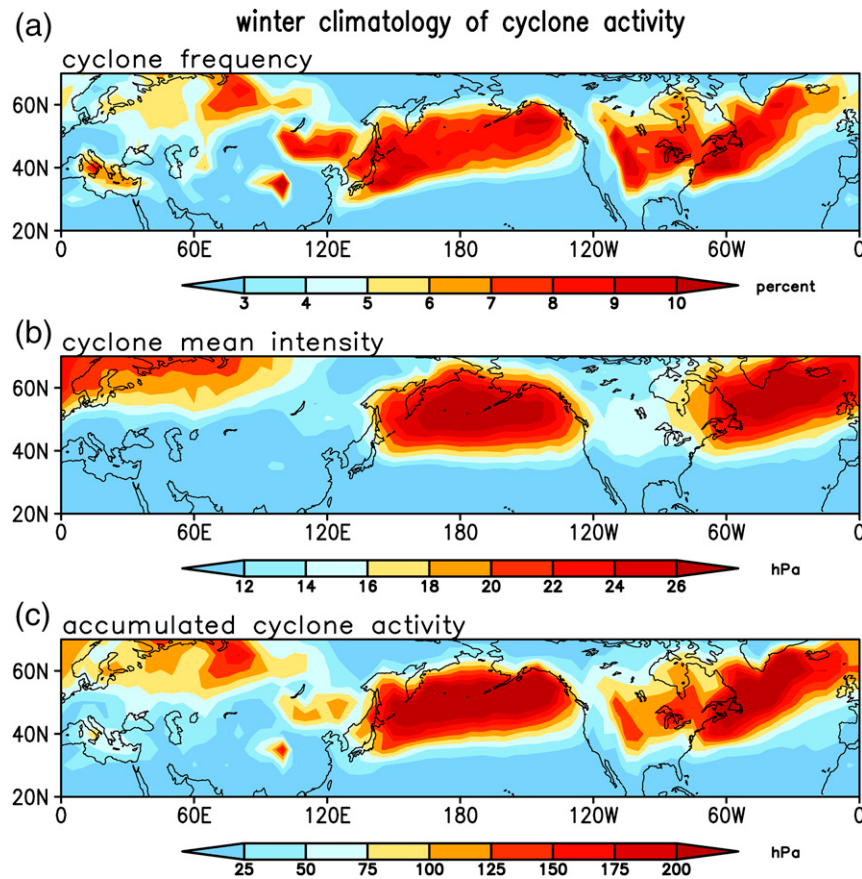


FIG. 4. Climatology of the Northern Hemisphere extratropical cyclone activity identified by an objective cyclone-tracking method and averaged during 1979–2014 boreal winter seasons (November–April). (a) Cyclone frequency (percent). (b) Cyclone mean intensity (hPa). (c) “Accumulated” cyclone activity (hPa).

For the cyclone mean intensity (Fig. 6), the anomalies are rather noisy and do not show much similarities to the MJO composites of pp anomalies (Fig. 3).

MJO modulation of the “accumulated” cyclone activity, which includes contributions from both cyclone frequency and intensity, is shown in Fig. 7. It is found that the anomalous cyclone activity indicated by this quantity shows great similarities to the MJO composited pp anomalies (Fig. 3), which is improved from the frequency or intensity alone. Note that while the anomalies shown in Fig. 7 do not pass a significance test at a 90% confidence level based on a two-tailed Student's *t* test, the large-scale enhancement and suppression of the storm tracks due to the MJO modulation depicted in Fig. 7 and those based on pp (Fig. 3) generally agree with each other, lending confidence to the results based on the cyclone-tracking method. Major features present in both methods can be summarized as follows. Strong variations are found over the North Pacific, extending through North America and the North Atlantic into northern Europe, with weak

anomalies over most of the Eurasian continent. The anomalous patterns are often characterized by meandering zonal bands although not as continuous as those in the meridional wind variance owing to stronger impacts of surface conditions, such as the Kuroshio Extension and the Rockies, with anomalies of opposite sign at one or both flanks. Overall, the positive-negative anomalies propagate eastward and slightly northward throughout the MJO cycle. For example, enhanced cyclone activity is first evident off of Japan and the Kuroshio Extension is in phase 3 and moves eastward through the central Pacific, reaching the northeast Pacific (phase 4–5), while reduced cyclone activity takes place over the area of Japan in phase 6 and moves northeast slowly, terminating in phase 8.

Comparing Fig. 7 to Figs. 5 and 6, we find that major contribution to the anomalies in the accumulated cyclone activity comes from the cyclone frequency anomalies, with eight-phase averaged pattern correlation between Fig. 5 and Fig. 7 over the NH ( $20^{\circ}$ – $70^{\circ}$ N) being 0.83. On the other hand, the averaged pattern correlation between the

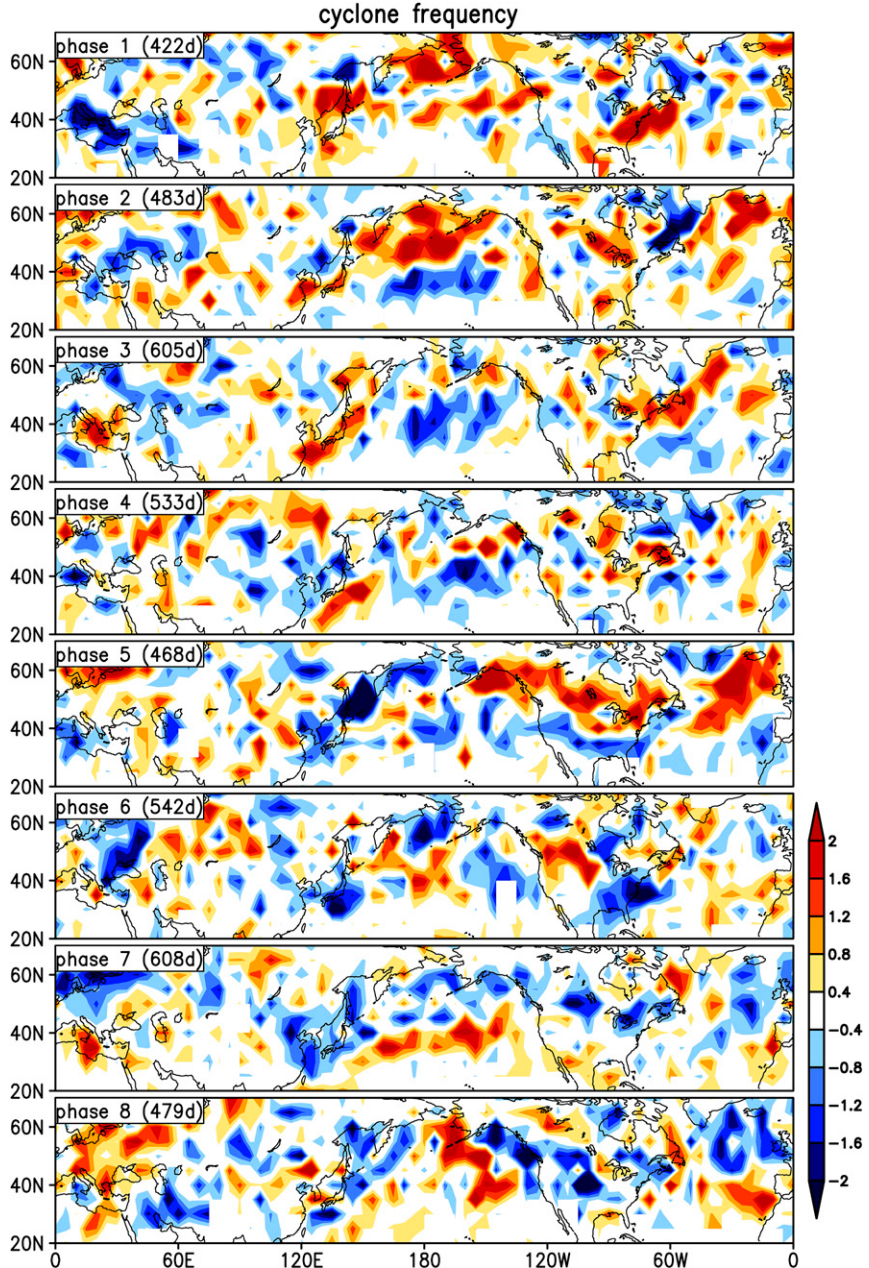


FIG. 5. (top to bottom) Eight-phase MJO composites of the cyclone frequency anomalies relative to the winter climatology (unitless). Only strong MJO days ( $\text{RMM1}^2 + \text{RMM2}^2 \geq 1$ ) during 1979–2014 winter seasons (November–April) are used for the composite, whose number for each phase is indicated at the upper-left corner of each panel.

mean intensity (Fig. 6) and accumulated activity (Fig. 7) decreases to 0.39.

Note that there is little correlation between the anomalous patterns of cyclone frequency and mean intensity (Fig. 5 vs Fig. 6), with the eight-phase mean correlation being 0.07. This means that a reduction–increase of cyclone frequency is not necessarily accompanied by a reduction–increase of the cyclone intensity, and vice

versa, which also suggests that it is not straightforward to translate the storm-track change in terms of eddy variance (one single value) to the cyclone statistics (several cyclone properties). For example, reduced eddy variance could be due to a reduction in either cyclone frequency or mean intensity, or both, or an even more complex situation: stronger reduction in one with a weaker increase in the other. Thus, the cyclone-tracking method provides

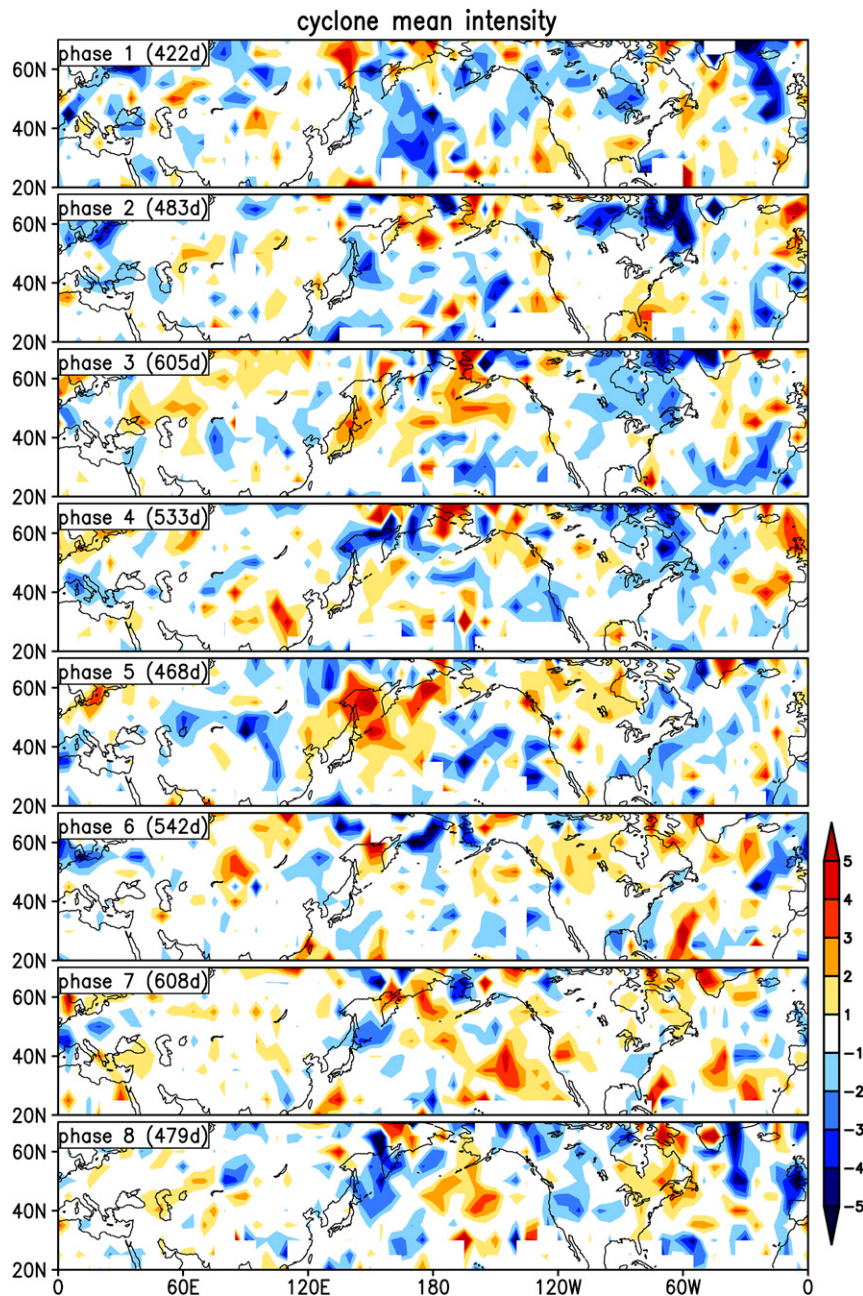


FIG. 6. As in Fig. 5, but for the cyclone mean intensity (hPa). No points are statistically significant at a 90% confidence level based on a two-tailed Student's *t* test, and thus no significance level is shown.

useful information that cannot be obtained based on the eddy variance method alone. On the other hand, results based on cyclone tracking are often noisy and barely pass the significance test, while those based on the eddy statistics are much more robust, lending an effective way to check the robustness of the cyclone-tracking results. Thus, these two methods are complementary to each other, providing more complete information when used

together for the same context such as the examination of MJO-induced variability.

## 5. Possible physical factors through which the MJO modulates the storm track

Results presented above have shown that the MJO exerts clear modulation on the NH storm tracks based

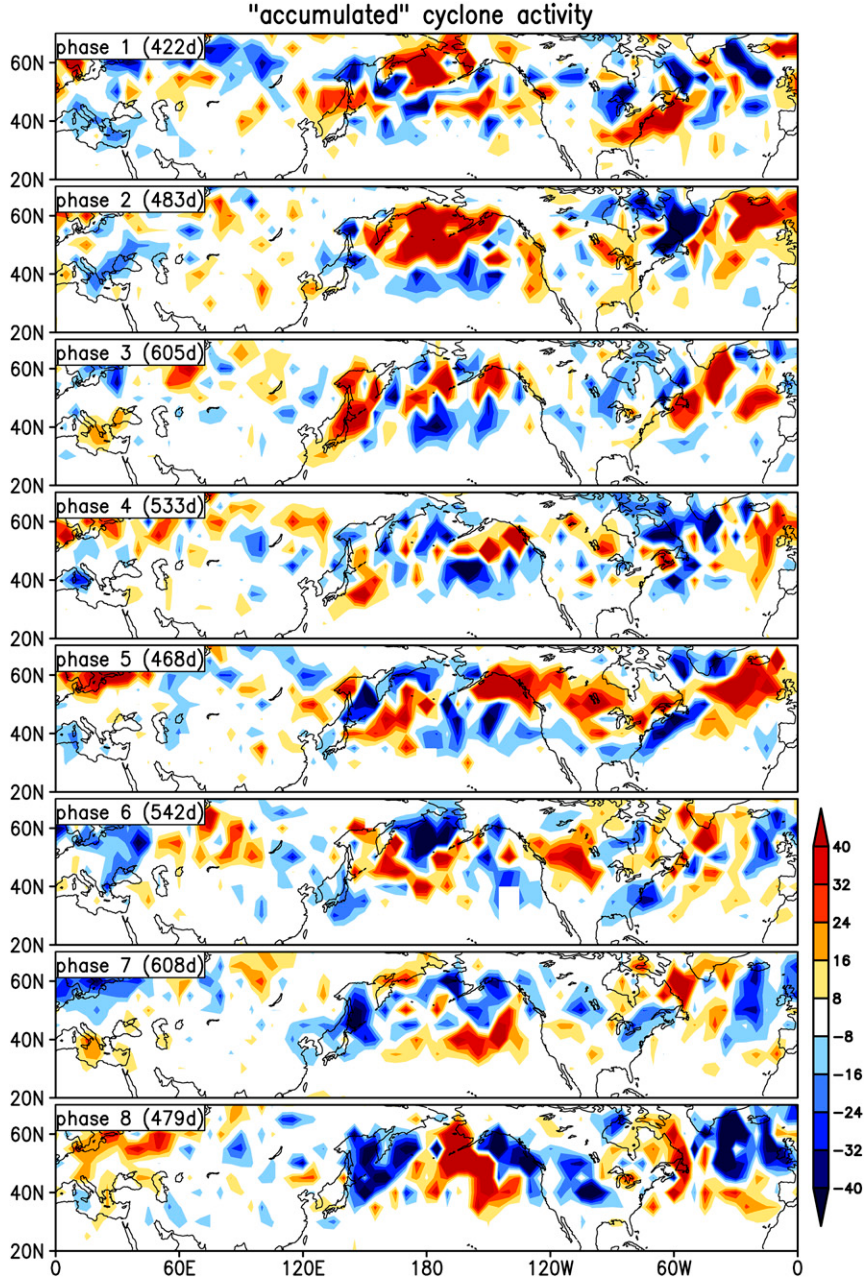


FIG. 7. As in Fig. 6, but for the “accumulated” cyclone activity (Pa).

on both eddy variance and cyclone-tracking methods. In this section, we will examine possible physical factors through which the MJO modulates the storm tracks.

#### *a. Mean flow and moisture anomalies associated with the MJO*

As mentioned in the introduction, anomalous tropical heating associated with the MJO can excite strong Rossby wave trains that propagate to the extratropics and alter the large-scale circulation as well as mean flow

there (e.g., Hoskins and Karoly 1981; Sardeshmukh and Hoskins 1988). The mean flow changes will then lead to changes in the baroclinic wave activity. At the same time, these baroclinic waves will feed back onto the mean flow. This is the well-known eddy-mean flow interaction (e.g., Andrews and McIntyre 1976; Hoskins et al. 1983; and many others). When considered under time scales longer than the eddy time scale (*in this case, the intraseasonal time scale*), the storm track and the mean flow are expected to exhibit a considerable

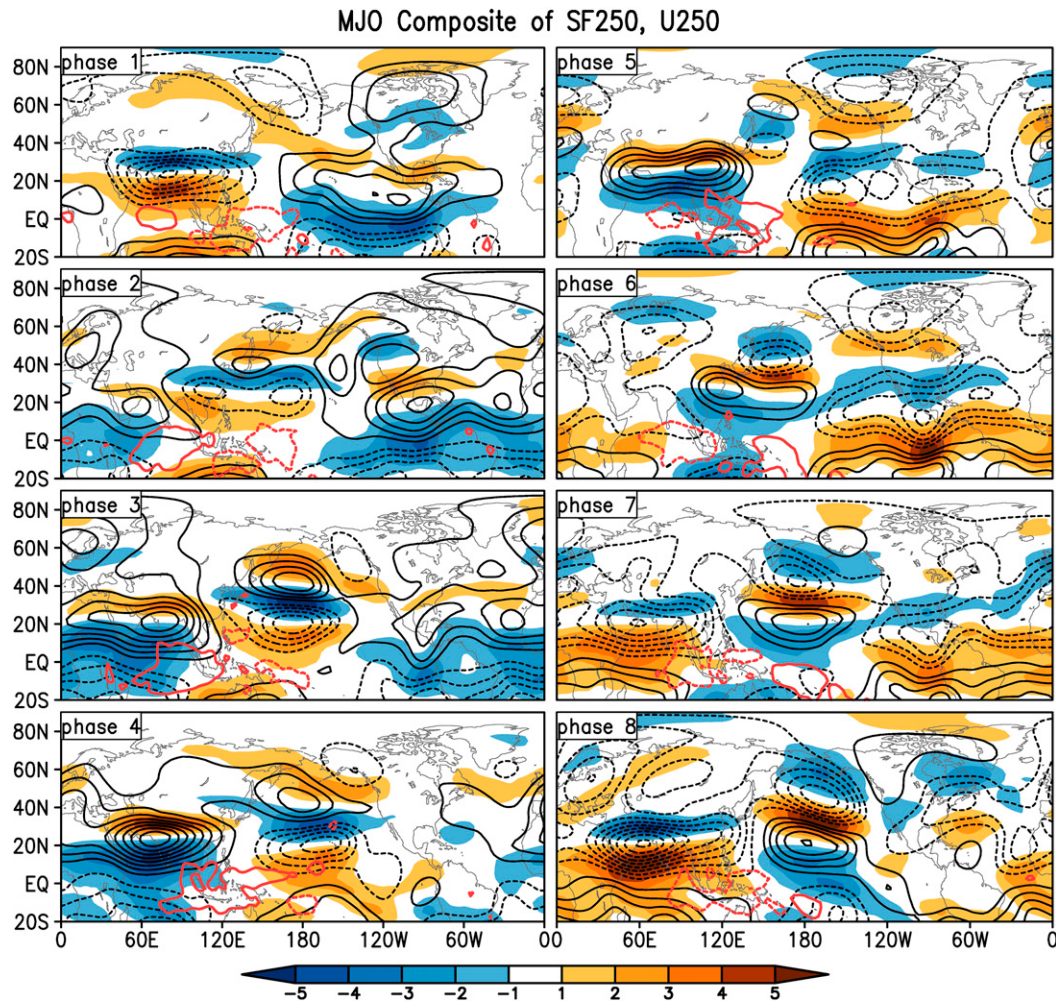


FIG. 8. Eight-phase MJO composites of 20–100-day filtered anomalies of 250-hPa streamfunction ( $\text{m}^2 \text{s}^{-1}$ ; black contours) and 250-hPa zonal wind ( $\text{m s}^{-1}$ ; color shading). The contour interval is  $10^6 \text{ m}^2 \text{s}^{-1}$  and the zero contour is omitted. Only strong MJO days ( $\text{RMM1}^2 + \text{RMM2}^2 \geq 1$ ) during 1979–2014 winter seasons (November–April) are used for the composite. Almost all the values at the points displayed are statistically significant at a 99% confidence level based on a two-tailed Student's *t* test, and thus no significance level is shown. Superimposed are the active (red solid contour) and suppressed (red dashed contour) MJO convection centers, which are indicated by the composites of the 20–100-day filtered precipitation anomalies with values of  $+1$  and  $-1 \text{ mm day}^{-1}$ , respectively, based on 1998–2012 TRMM data.

amount of covariations. This has also been described as the “**symbiotic**” relationship between the mean flow and the storm track in previous studies (e.g., Lau 1988; Cai and Mak 1990). Thus, we will first examine the MJO-related mean flow anomalies as a possible physical factor through which the MJO modulates the storm tracks.

The MJO composites of the intraseasonal (20–100 day) filtered anomalies of 250-hPa zonal wind (U250) during 1979–2014 winters are shown for the entire tropics and the NH in Fig. 8 (shading). The 250-hPa streamfunction (contours) is also shown in order to demonstrate the large-scale circulation response to the MJO convection. Note that the locations of the active and suppressed MJO

convection centers are marked by the red solid and dashed contours, which correspond to the 20–100-day filtered precipitation anomalies of  $+1$  and  $-1 \text{ mm day}^{-1}$ , respectively, based on 1998–2012 TRMM data. As expected, the upper-level circulation response to the MJO convection is characterized by Rossby wave trains propagating from the subtropics into the higher latitudes and then turning back toward the lower latitudes with alternative positive and negative anomalous centers. However, because the MJO heating is not a single localized source but a dipole of enhanced and suppressed anomalies evolving in both space and time, the circulation response is not as simple as that predicted

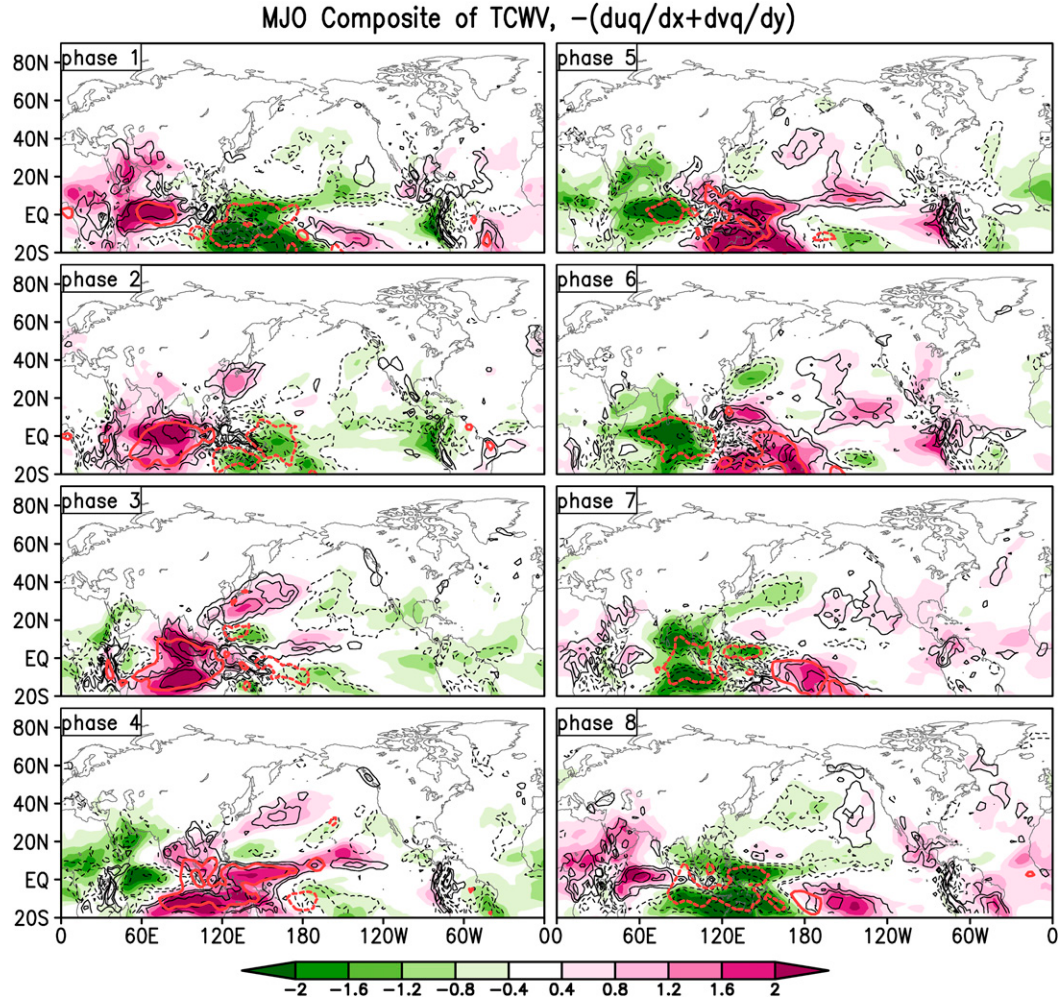


FIG. 9. As in Fig. 8, except that the shading is the TCWV ( $\text{kg m}^{-2}$ ) and the contour is the horizontal water vapor convergence integrated from 1000 to 500 hPa (interval:  $1 \text{ kg m}^{-1}$ ) calculated from specific humidity and horizontal winds. Almost all the values at the points displayed are statistically significant at a 99% confidence level based on a two-tail Student's *t* test, thus no significance level is shown.

by the Gill (1980) model. Nevertheless, the major features still resemble what is described by the Rossby wave dispersion theory (Hoskins and Karoly 1981). For example, associated with enhanced MJO convection (red solid contour) and lower-tropospheric convergence, a lower-level Rossby gyre with cyclonic anomalous circulation occurs at the northwest side of the heating (not shown). Meanwhile, an anticyclonic anomalous circulation occurs at the upper level corresponding to upper-level divergence. Subsequently, this upper-level divergence will lead to the convergence anomaly at higher latitude, which gives rise to the next divergence anomaly, forming a train of Rossby waves propagating roughly along a great circle. This is the case for phases 4, 5, 6, and 7. Conversely, the upper-level Rossby wave train starts with a cyclonic circulation in the subtropics

to the northwest of the suppressed MJO convection, which is evident in phases 8, 1, 2, and 3. Accompanied with the circulation anomalies discussed above, the response of the zonal wind to the MJO convection anomalies is manifested as alternating westerly and easterly anomalies. These features are consistent with those of previous observational and modeling studies (Ferranti et al. 1990; Matthews and Meredith 2004; Cassou 2008; Lin et al. 2009; Seo and Son 2012; among many others).

In addition to the mean flow anomalies, the MJO-associated TCWV anomalies are also shown (shading in Fig. 9) since results below suggest that the moisture variations might also contribute to the observed storm-track variations. Figure 9 shows that within the tropics, positive TCWV anomalies generally occur in the vicinity

of enhanced MJO convection, while negative anomalies occur near suppressed convection. The anomalies of the TCWV are not confined within the tropics but also extend to the midlatitudes, reaching up to 40°N. Pronounced moisture anomalies are found over the North Pacific, particularly over its western boundary (i.e., Kuroshio and Kuroshio Extension region), as well as over the central North Pacific. In addition, the intraseasonal anomalies of the horizontal convergence of water vapor integrated from 1000 to 500 hPa are examined (contours in Fig. 9), which are generally collocated with the TCWV anomalies.

#### b. Modulation of storm tracks by the mean flow and moisture variations

Given the close relationship between the storm track and mean flow discussed in the preceding subsection, we first compare the MJO-associated U250 anomalies (black contours) to the anomalies of the storm track indicated by vv250 (shading) to explore how much variations in the storm track might be explained by the mean flow change (Fig. 10). Note that in this subsection only the results with the storm track indicated by vv250 are shown; however, similar conclusions are also obtained from the analysis of pp. We focus on the North Pacific to the North Atlantic region (120°–60°E) since the storm-track response to the MJO is very weak over the Eurasian continent (Fig. 2).

Generally there is consistency between the storm-track and mean flow variations, especially over the region north of 40°N: an enhanced storm track is often accompanied by westerly anomalies, while a reduced storm track is accompanied by easterly anomalies, consistent with the results of Lau (1988). The pattern correlation between the storm track and mean flow anomalies averaged over eight MJO phases is about 0.5 for the region of 120°–60°E (from 120°E all the way westward to 60°E, passing 0°) and 40°–70°N, which is significant at a 99% confidence level based on a two-tailed Student's *t* test. Some inconsistency between the storm-track and mean flow variations can also be noticed. For example, the storm-track anomalies are generally displaced southward from the mean flow anomalies. This might suggest that other physical processes (e.g., barotropic conversion) than the baroclinic conversion also play important roles in generating the observed storm-track anomalies. Nevertheless, the strong correlation between the storm track and mean flow anomalies indicates that over the region north of 40°N the MJO modulates the storm track mainly through the modulation of the mean flow.

The situation over the subtropics is quite different from that in the higher latitudes: the mean flow variations are strong over the west to central Pacific, while the storm-track variations are very weak, nearly indiscernible.

One might argue that this could be due to the fact that the climatological storm track is much weaker over the subtropics compared to that in the midlatitudes. However, this should not be the main reason since large storm-track variations are still found over the central to east Pacific of same latitudes. Here, we speculate that the moisture might be another physical factor that needs to be taken into account in order to explain the storm-track variations in the subtropics. We hypothesize that positive moisture anomaly corresponds to stronger storm-track activity (e.g., Chang and Zurita-Gotor 2007). On the one hand, increased moisture supply can invigorate the cyclones through enhanced diabatic heating in the rising warm air ahead of the cyclones (e.g., Gutowski et al. 1992); in addition, increased lower- to midtroposphere moisture decreases the effective static instability (Emmanuel et al. 1987). Figure 10 shows that over the west to central Pacific, the mean flow anomalies are usually accompanied with moisture anomalies of opposite sign. Thus, the contributions from the mean flow and moisture supply anomalies may often counteract each other, leaving little storm-track change over this region. In contrast, over the central to eastern Pacific, the mean flow and moisture anomalies often have same signs, possibly resulting in quite strong storm-track variations.

These results are further demonstrated in Fig. 11, in which we show vv250, U250, and TCWV anomalies in each MJO phase averaged over two representative regions. One region is the North Pacific north of 40°N (40°–60°N, 140°–200°E), and the other is the subtropical west to central Pacific (25°–40°N, 120°E–180°). The MJO cycle of the averages over the first region shows that the storm-track variations mainly covary with the mean flow changes, while the potentially counteracting effects between the mean flow and tropospheric moisture content can be found in the second region.

It should be pointed out that results in this part are based on simple correlation analysis, which indeed does not guarantee the causality. Although the role of the mean flow in modulating the storm track has strong theoretical and empirical support, the relationship between moisture and storm-track variations is still rather poorly understood (e.g., Chang and Zurita-Gotor 2007; Xia and Chang 2014). More detailed diagnostics or modeling studies regarding the physical mechanisms through which the MJO modulates the storm tracks are thus desirable in the future.

## 6. Conclusions and discussion

In this study, the intraseasonal variations of the NH storm track associated with the MJO have been investigated using 36 yr (1979–2014) of extended boreal

### MJO Composite of vv250, U250 & TCWV

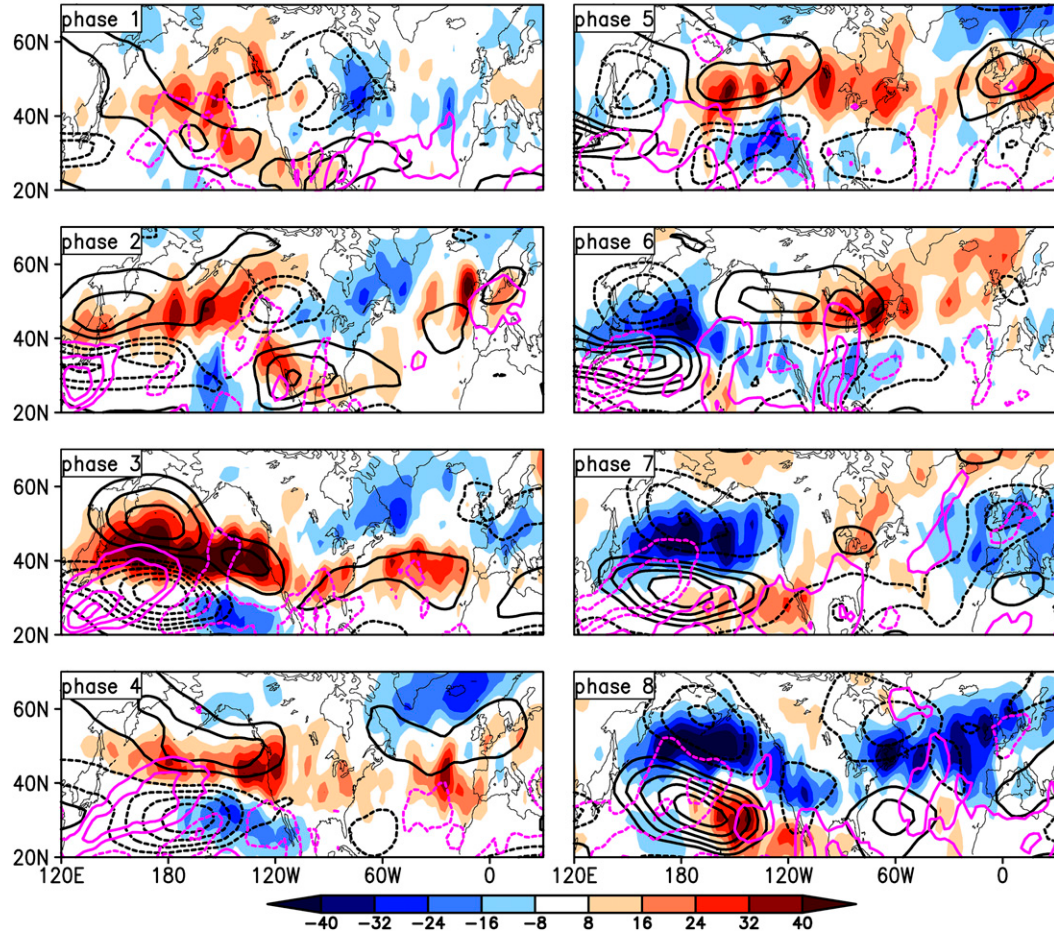


FIG. 10. Eight-phase MJO composites of the intraseasonal (20–100 day) filtered anomalies of the storm track quantified by vv250 ( $\text{m}^2 \text{s}^{-2}$ ; shading), U250 ( $\text{m s}^{-1}$ ; black contours), and TCWV ( $\text{kg m}^{-2}$ ; purple contours), which are identical to the shadings shown in Figs. 2, 8, and 9, respectively. Only strong MJO days ( $\text{RMM1}^2 + \text{RMM2}^2 \geq 1$ ) during 1979–2014 winter seasons (November–April) are used for the composite. For all three quantities, almost all the points displayed are significant at a 99% confidence level based on a two-tailed Student's *t* test, and thus no significance contour is shown.

winter (November–April) data from ERA-Interim. There are two basic methods to quantify the storm track: one is based on the Eulerian eddy statistics, and the other based on the Lagrangian cyclone-tracking statistics. Previous studies generally focused on one approach. In this study, we have examined the results based on both methods such that more insights on the intraseasonal variability of the NH storm track can be obtained.

The intraseasonal (20–100 day) filtered vv250 are first composited through eight MJO phases using the WH MJO RMM index. The MJO composites of vv250 are characterized by a zonal band of strong positive (or negative) anomalies over about  $35^\circ$ – $55^\circ\text{N}$ , which meander from the Pacific, across North America and the

Atlantic, and into northern Europe, and are accompanied by weaker anomalies of opposite sign at one or both flanks. The storm-track anomalies move eastward and northward along with the eastward propagation of the MJO convection anomalies. These features are generally consistent with what is depicted in previous studies (DJ11 and LL12). The results based on pp are consistent overall with those based on vv250 but exhibit larger zonal variations with the anomalies more prominent over the western boundary of oceans and discontinuous over the Rocky Mountains. This could be due to the stronger influence of the earth's surface, such as the Kuroshio Extension and the Rocky Mountains on the storm track; an influence more-based on a surface parameter than on an upper-level one.

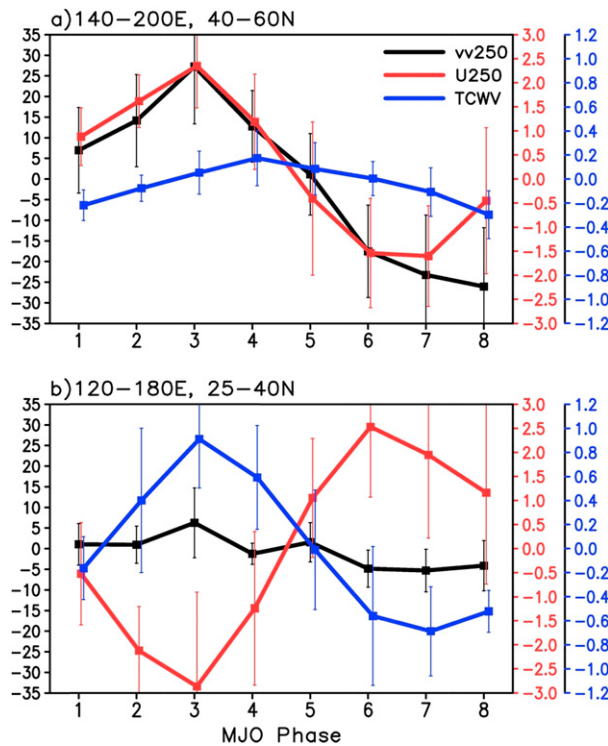


FIG. 11. The eight-phase MJO cycle of the domain-averaged intraseasonal anomalies of the storm track quantified by the 24-h-difference variance of 250-hPa meridional wind ( $\text{m}^2 \text{s}^{-2}$ ; black), 250-hPa zonal wind ( $\text{m s}^{-1}$ ; red), and TCWV ( $\text{kg m}^{-2}$ ; blue) over (a)  $40^{\circ}$ – $60^{\circ}$ N,  $140^{\circ}$ – $200^{\circ}$ E and (b)  $25^{\circ}$ – $40^{\circ}$ N,  $120^{\circ}$ E– $180^{\circ}$  in Fig. 10. The error bars denote the 99% confidence level of the means based on a two-tailed Student's *t* test.

The cyclones identified as the surface pressure minima were then tracked. The results based on the cyclone-tracking method are overall noisy. Despite the level of noise, the MJO composites of the cyclone frequency anomalies relative to the winter climatology exhibit systematic variations that bear considerable similarities to the MJO composites of pp anomalies. The mean cyclone intensity does not show as strong systematic changes associated with the evolution of the MJO as the cyclone frequency. Nevertheless, when a quantity that takes into account both the cyclone frequency and mean intensity (i.e., the product of the cyclone frequency and mean intensity, which we call the “accumulated” cyclone activity) is introduced, the consistency between the MJO composites of the accumulated cyclone activity and those of pp becomes evident. The introduction of accumulated cyclone activity is novel, and our results suggest that it is a more appropriate quantity to be compared with the eddy variance than the frequency or intensity alone, which could be of important use in future study. In addition, our results suggest that the use of the same meteorological parameter in both the

cyclone-tracking and eddy variance methods might be necessary since certain differences are found between vv250 and pp, and the cyclone statistics by tracking MSLP minima are more comparable to the latter. The adoption of the accumulated cyclone activity and direct comparison to pp might both help explain the better consistency found in our study than that by Grise13, in which the 850-hPa vorticity is tracked and compared to the EKE.

As we have shown, the cyclone-tracking method provides useful information such as cyclone frequency and mean intensity that cannot be obtained from the eddy statistics alone. However, results based on cyclone tracking are often noisy and barely pass the significance test, while those based on the eddy statistics are generally much clearer, providing an effective way to confirm the robustness of the cyclone-tracking results. Thus, the use of both methods together is often desirable.

Finally, possible physical factors through which the MJO modulates the storm track have been briefly discussed. It is found that overall the storm-track variations can be largely attributed to the MJO-associated mean flow change, especially in the region north of  $40^{\circ}$ N: an enhanced storm track is often accompanied by the westerly anomalies, while a reduced storm track is often accompanied by the easterly anomalies. In the subtropics, it appears that moisture variations may need to be considered in order to explain the observed storm-track variations. It should be noted that our results are purely diagnostic. The relationships between the intra-seasonal variations in the storm track and the mean flow and tropospheric moisture have only been examined through correlation and composite analyses. Further studies, including numerical simulations using an idealized storm-track model (Chang 2001; Chang and Guo 2007) or more comprehensive GCMs, are needed to explore the details of the identified MJO–storm-track interactions.

Our results indicate that the MJO exerts clear modulations of the midlatitude storm track through large-scale dynamic and thermodynamic variations associated with the MJO convection anomalies. Given the close relationship between the storm track and midlatitude weather as well as the fact that the MJO is the major source of predictability on the intraseasonal time scale, the results of this study suggest that there is potential predictability of the weather–climate variability in the extratropics through MJO’s impact on the extratropics.

**Acknowledgments.** The authors thank George Kiladis and two anonymous reviewers for constructive comments that helped improve this paper greatly. This work was supported by NSF Grant AGS-1347132 and NOAA Grant NA15OAR431074. EC was supported by NOAA Grant NA16OAR4310070.

## REFERENCES

- Andrews, D., and M. McIntyre, 1976: Planetary waves in horizontal and vertical shear: The generalized Eliassen-Palm relation and the mean zonal acceleration. *J. Atmos. Sci.*, **33**, 2031–2048, doi:[10.1175/1520-0469\(1976\)033<2031:PWIHAV>2.0.CO;2](https://doi.org/10.1175/1520-0469(1976)033<2031:PWIHAV>2.0.CO;2).
- Bell, G. D., and L. F. Bosart, 1989: A 15-year climatology of Northern Hemisphere 500 mb closed cyclone and anticyclone centers. *Mon. Wea. Rev.*, **117**, 2142–2164, doi:[10.1175/1520-0493\(1989\)117<2142:AYCONH>2.0.CO;2](https://doi.org/10.1175/1520-0493(1989)117<2142:AYCONH>2.0.CO;2).
- Blackmon, M. L., 1976: A climatological spectral study of the 500-mb geopotential height of the Northern Hemisphere. *J. Atmos. Sci.*, **33**, 1607–1623, doi:[10.1175/1520-0469\(1976\)033<1607:ACSSOT>2.0.CO;2](https://doi.org/10.1175/1520-0469(1976)033<1607:ACSSOT>2.0.CO;2).
- , J. M. Wallace, N. C. Lau, and S. L. Mullen, 1977: An observational study of the Northern Hemisphere wintertime circulation. *J. Atmos. Sci.*, **34**, 1040–1053, doi:[10.1175/1520-0469\(1977\)034<1040:AOSOTN>2.0.CO;2](https://doi.org/10.1175/1520-0469(1977)034<1040:AOSOTN>2.0.CO;2).
- Booth, J., L. Thompson, J. Patoux, K. Kelly, and S. Dickinson, 2010: The signature of the midlatitude tropospheric storm tracks in the surface winds. *J. Climate*, **23**, 1160–1174, doi:[10.1175/2009JCLI3064.1](https://doi.org/10.1175/2009JCLI3064.1).
- Businger, S., T. M. Graziano, M. L. Kaplan, and R. A. Rozumalski, 2005: Cold-air cyclogenesis along the Gulf Stream front: Investigation of diabatic impacts on cyclone development, frontal structure, and track. *Meteor. Atmos. Phys.*, **88**, 65–90, doi:[10.1007/s00703-003-0050-y](https://doi.org/10.1007/s00703-003-0050-y).
- Cai, M., and M. Mak, 1990: Symbiotic relation between planetary and synoptic-scale waves. *J. Atmos. Sci.*, **47**, 2953–2968, doi:[10.1175/1520-0469\(1990\)047<2953:SRBPAS>2.0.CO;2](https://doi.org/10.1175/1520-0469(1990)047<2953:SRBPAS>2.0.CO;2).
- Cassou, C., 2008: Intraseasonal interaction between the Madden-Julian oscillation and the North Atlantic Oscillation. *Nature*, **455**, 523–527, doi:[10.1038/nature07286](https://doi.org/10.1038/nature07286).
- Chang, E. K. M., 2001: GCM and observational diagnoses of the seasonal and interannual variations of the Pacific storm track during the cool season. *J. Atmos. Sci.*, **58**, 1784–1800, doi:[10.1175/1520-0469\(2001\)058<1784:GAODOT>2.0.CO;2](https://doi.org/10.1175/1520-0469(2001)058<1784:GAODOT>2.0.CO;2).
- , 2014: Impacts of background field removal on CMIP5 projected changes in Pacific winter cyclone activity. *J. Geophys. Res. Atmos.*, **119**, 4626–4639, doi:[10.1002/2013JD020746](https://doi.org/10.1002/2013JD020746).
- , and Y. Guo, 2007: Dynamics of the stationary anomalies associated with the interannual variability of the midwinter Pacific storm track—The roles of tropical heating and remote eddy forcing. *J. Atmos. Sci.*, **64**, 2442–2461, doi:[10.1175/JAS3986.1](https://doi.org/10.1175/JAS3986.1).
- , and P. Zurita-Gotor, 2007: Simulating the seasonal cycle of the Northern Hemisphere storm tracks using idealized nonlinear storm-track models. *J. Atmos. Sci.*, **64**, 2309–2331, doi:[10.1175/JAS3957.1](https://doi.org/10.1175/JAS3957.1).
- Dee, D. P., and Coauthors, 2011: The ERA-Interim reanalysis: Configuration and performance of the data assimilation system. *Quart. J. Roy. Meteor. Soc.*, **137**, 553–597, doi:[10.1002/qj.828](https://doi.org/10.1002/qj.828).
- Deng, Y., and T. Jiang, 2011: Intraseasonal modulation of the North Pacific storm track by tropical convection in boreal winter. *J. Climate*, **24**, 1122–1137, doi:[10.1175/2010JCLI3676.1](https://doi.org/10.1175/2010JCLI3676.1).
- Donohoe, A., and D. S. Battisti, 2009: The amplitude asymmetry between synoptic cyclones and anticyclones: Implications for filtering methods in feature tracking. *Mon. Wea. Rev.*, **137**, 3874–3887, doi:[10.1175/2009MWR2837.1](https://doi.org/10.1175/2009MWR2837.1).
- Emanuel, K. A., M. Fantini, and A. J. Thorpe, 1987: Baroclinic instability in an environment of small stability to slantwise moist convection. Part I: Two-dimensional models. *J. Atmos. Sci.*, **44**, 1559–1573, doi:[10.1175/1520-0469\(1987\)044<1559:BIIAEQ>2.0.CO;2](https://doi.org/10.1175/1520-0469(1987)044<1559:BIIAEQ>2.0.CO;2).
- Ferranti, L., T. N. Palmer, F. Molteni, and K. Klinker, 1990: Tropical-extratropical interaction associated with the 30–60 day oscillation and its impact on medium and extended range prediction. *J. Atmos. Sci.*, **47**, 2177–2199, doi:[10.1175/1520-0469\(1990\)047<2177:TEIAWT>2.0.CO;2](https://doi.org/10.1175/1520-0469(1990)047<2177:TEIAWT>2.0.CO;2).
- Gill, A. E., 1980: Some simple solutions for heat-induced tropical circulation. *Quart. J. Roy. Meteor. Soc.*, **106**, 447–462, doi:[10.1002/qj.49710644905](https://doi.org/10.1002/qj.49710644905).
- Grise, K. M., S.-W. Son, and J. R. Gyakum, 2013: Intraseasonal and interannual variability in North American storm tracks and its relationship to equatorial Pacific variability. *Mon. Wea. Rev.*, **141**, 3610–3625, doi:[10.1175/MWR-D-12-00322.1](https://doi.org/10.1175/MWR-D-12-00322.1).
- Gutowski, W. J., L. W. Branscome, and D. A. Stewart, 1992: Live cycles of moist baroclinic eddies. *J. Atmos. Sci.*, **49**, 306–319, doi:[10.1175/1520-0469\(1992\)049<0306:LCOMBE>2.0.CO;2](https://doi.org/10.1175/1520-0469(1992)049<0306:LCOMBE>2.0.CO;2).
- Henderson, S., E. Maloney, and E. Barnes, 2016: The influence of the Madden-Julian oscillation on Northern Hemisphere winter blocking. *J. Climate*, **29**, 4597–4616, doi:[10.1175/JCLI-D-15-0502.1](https://doi.org/10.1175/JCLI-D-15-0502.1).
- Hodges, K. I., 1994: A general method for tracking analysis and its application to meteorological data. *Mon. Wea. Rev.*, **122**, 2573–2586, doi:[10.1175/1520-0493\(1994\)122<2573:AGMFTA>2.0.CO;2](https://doi.org/10.1175/1520-0493(1994)122<2573:AGMFTA>2.0.CO;2).
- , 1995: Feature tracking on the unit sphere. *Mon. Wea. Rev.*, **123**, 3458–3465, doi:[10.1175/1520-0493\(1995\)123<3458:FTOTUS>2.0.CO;2](https://doi.org/10.1175/1520-0493(1995)123<3458:FTOTUS>2.0.CO;2).
- , 1999: Adaptive constraints for feature tracking. *Mon. Wea. Rev.*, **127**, 1362–1373, doi:[10.1175/1520-0493\(1999\)127<1362:ACFFT>2.0.CO;2](https://doi.org/10.1175/1520-0493(1999)127<1362:ACFFT>2.0.CO;2).
- Horel, J. D., and J. M. Wallace, 1981: Planetary scale atmospheric phenomena associated with the Southern Oscillation. *Mon. Wea. Rev.*, **109**, 813–829, doi:[10.1175/1520-0493\(1981\)109<0813:PSAPAW>2.0.CO;2](https://doi.org/10.1175/1520-0493(1981)109<0813:PSAPAW>2.0.CO;2).
- Hoskins, B. J., and D. J. Karoly, 1981: The steady linear response of a spherical atmosphere to thermal and orographic forcing. *J. Atmos. Sci.*, **38**, 1179–1196, doi:[10.1175/1520-0469\(1981\)038<1179:TSLROA>2.0.CO;2](https://doi.org/10.1175/1520-0469(1981)038<1179:TSLROA>2.0.CO;2).
- , and P. J. Valdes, 1990: On the existence of storm-tracks. *J. Atmos. Sci.*, **47**, 1854–1864, doi:[10.1175/1520-0469\(1990\)047<1854:OTEOST>2.0.CO;2](https://doi.org/10.1175/1520-0469(1990)047<1854:OTEOST>2.0.CO;2).
- , and K. I. Hodges, 2002: New perspectives on the Northern Hemisphere winter storm tracks. *J. Atmos. Sci.*, **59**, 1041–1061, doi:[10.1175/1520-0469\(2002\)059<1041:NPOTNH>2.0.CO;2](https://doi.org/10.1175/1520-0469(2002)059<1041:NPOTNH>2.0.CO;2).
- , I. N. James, and G. H. White, 1983: The shape, propagation and mean-flow interaction of large-scale weather systems. *J. Atmos. Sci.*, **40**, 1595–1612, doi:[10.1175/1520-0469\(1983\)040<1595:TSPAMF>2.0.CO;2](https://doi.org/10.1175/1520-0469(1983)040<1595:TSPAMF>2.0.CO;2).
- Hsu, H. H., 1996: Global view of the intraseasonal oscillation during northern winter. *J. Climate*, **9**, 2386–2406, doi:[10.1175/1520-0442\(1996\)009<2386:GVOTIO>2.0.CO;2](https://doi.org/10.1175/1520-0442(1996)009<2386:GVOTIO>2.0.CO;2).
- Huffman, G. J., and Coauthors, 2007: The TRMM Multisatellite Precipitation Analysis (TMPA): Quasi-global, multiyear, combined-sensor precipitation estimates at fine scales. *J. Hydrometeorol.*, **8**, 38–55, doi:[10.1175/JHM560.1](https://doi.org/10.1175/JHM560.1).
- Joyce, T. M., Y. O. Kwon, and L. Yu, 2009: On the relationship between synoptic wintertime atmospheric variability and path shifts in the Gulf Stream and the Kuroshio Extension. *J. Climate*, **22**, 3177–3192, doi:[10.1175/2008JCLI2690.1](https://doi.org/10.1175/2008JCLI2690.1).
- Kiladis, G. N., J. Dias, K. H. Straub, M. C. Wheeler, S. N. Tulich, K. Kikuchi, K. M. Weickmann, and M. J. Ventrice, 2014: A comparison of OLR and circulation-based indices for tracking the MJO. *Mon. Wea. Rev.*, **142**, 1697–1715, doi:[10.1175/MWR-D-13-00301.1](https://doi.org/10.1175/MWR-D-13-00301.1).

- Klein, W. H., 1957: Principal tracks and mean frequencies of cyclones and anticyclones in the Northern Hemisphere. U.S. Weather Bureau Research Paper 40, 60 pp.
- Knutson, T. R., and K. L. Weickmann, 1987: 30–60 day atmospheric oscillations: Composite life cycles of convection and circulation anomalies. *Mon. Wea. Rev.*, **115**, 1407–1435, doi:[10.1175/1520-0493\(1987\)115<1407:DAOCLC>2.0.CO;2](https://doi.org/10.1175/1520-0493(1987)115<1407:DAOCLC>2.0.CO;2).
- Lau, K.-M., and T. J. Phillips, 1986: Coherent fluctuations of extratropical geopotential height and tropical convection in intraseasonal timescales. *J. Atmos. Sci.*, **43**, 1164–1181, doi:[10.1175/1520-0469\(1986\)043<1164:CFOFGH>2.0.CO;2](https://doi.org/10.1175/1520-0469(1986)043<1164:CFOFGH>2.0.CO;2).
- Lau, N.-C., 1988: Variability of the observed midlatitude storm tracks in relation to low-frequency changes in the circulation pattern. *J. Atmos. Sci.*, **45**, 2718–2743, doi:[10.1175/1520-0469\(1988\)045<2718:VOTOMS>2.0.CO;2](https://doi.org/10.1175/1520-0469(1988)045<2718:VOTOMS>2.0.CO;2).
- Lee, Y.-Y., and G.-H. Lim, 2012: Dependency of the North Pacific winter storm tracks on the zonal distribution of MJO convection. *J. Geophys. Res.*, **117**, D14101, doi:[10.1029/2011JA017246](https://doi.org/10.1029/2011JA017246).
- Leith, C. E., 1973: The standard error of time-average estimates of climatic means. *J. Appl. Meteor.*, **12**, 1066–1068, doi:[10.1175/1520-0450\(1973\)012<1066:TSEOTA>2.0.CO;2](https://doi.org/10.1175/1520-0450(1973)012<1066:TSEOTA>2.0.CO;2).
- Liebmann, B., and D. L. Hartmann, 1984: An observational study of tropical–midlatitude interaction on intraseasonal time scales during winter. *J. Atmos. Sci.*, **41**, 3333–3350, doi:[10.1175/1520-0469\(1984\)041<3333:ASOTSI>2.0.CO;2](https://doi.org/10.1175/1520-0469(1984)041<3333:ASOTSI>2.0.CO;2).
- Lim, E.-P., and I. Simmonds, 2002: Explosive cyclone development in the Southern Hemisphere and a comparison with Northern Hemisphere events. *Mon. Wea. Rev.*, **130**, 2188–2209, doi:[10.1175/1520-0493\(2002\)130<2188:ECDITS>2.0.CO;2](https://doi.org/10.1175/1520-0493(2002)130<2188:ECDITS>2.0.CO;2).
- Lin, H., G. Brunet, and J. Derome, 2009: An observed connection between the North Atlantic Oscillation and the Madden–Julian oscillation. *J. Climate*, **22**, 364–380, doi:[10.1175/2008JCLI2515.1](https://doi.org/10.1175/2008JCLI2515.1).
- , —, and J. Fontecilla, 2010: Impact of the Madden–Julian oscillation on the intraseasonal forecast skill of the North Atlantic Oscillation. *Geophys. Res. Lett.*, **37**, L19803, doi:[10.1029/2010GL044315](https://doi.org/10.1029/2010GL044315).
- Madden, R., and P. Julian, 1971: Detection of a 40–50 day oscillation in the zonal wind in the tropical Pacific. *J. Atmos. Sci.*, **28**, 702–708, doi:[10.1175/1520-0469\(1971\)028<0702:DOADOI>2.0.CO;2](https://doi.org/10.1175/1520-0469(1971)028<0702:DOADOI>2.0.CO;2).
- , —, 1972: Description of global-scale circulation cells in the tropics with a 40–50 day period. *J. Atmos. Sci.*, **29**, 1109–1123, doi:[10.1175/1520-0469\(1972\)029<1109:DGSCC>2.0.CO;2](https://doi.org/10.1175/1520-0469(1972)029<1109:DGSCC>2.0.CO;2).
- Matthews, A. J., and G. N. Kiladis, 1999: The tropical–extratropical interaction between high-frequency transients and the Madden–Julian oscillation. *Mon. Wea. Rev.*, **127**, 661–677, doi:[10.1175/1520-0493\(1999\)127<0661:TTEIBH>2.0.CO;2](https://doi.org/10.1175/1520-0493(1999)127<0661:TTEIBH>2.0.CO;2).
- , and M. P. Meredith, 2004: Variability of Antarctic circumpolar transport and the southern annual mode associated with the Madden–Julian oscillation. *Geophys. Res. Lett.*, **31**, L24312, doi:[10.1029/2004GL021666](https://doi.org/10.1029/2004GL021666).
- Murray, R. J., and I. Simmonds, 1991: A numerical scheme for tracking cyclone centres from digital data. Part I: Development and operation of the scheme. *Aust. Meteor. Mag.*, **39**, 155–166.
- Nakamura, H., T. Sampe, A. Goto, W. Ohfuchi, and S.-P. Xie, 2008: On the importance of midlatitude oceanic frontal zones for the mean state and dominant variability in the tropospheric circulation. *Geophys. Res. Lett.*, **35**, L15709, doi:[10.1029/2008GL034010](https://doi.org/10.1029/2008GL034010).
- , A. Nishina, and S. Minobe, 2012: Response of storm tracks to bimodal Kuroshio path states south of Japan. *J. Climate*, **25**, 7772–7779, doi:[10.1175/JCLI-D-12-00326.1](https://doi.org/10.1175/JCLI-D-12-00326.1).
- O'Reilly, C. H., and A. Czaja, 2015: The response of the Pacific storm track and atmospheric circulation to Kuroshio Extension variability. *Quart. J. Roy. Meteor. Soc.*, **141**, 52–66, doi:[10.1002/qj.2334](https://doi.org/10.1002/qj.2334).
- Sardeshmukh, P. D., and B. J. Hoskins, 1988: The generation of global rotational flow by steady idealized tropical divergence. *J. Atmos. Sci.*, **45**, 1228–1251, doi:[10.1175/1520-0469\(1988\)045<1228:TGOGRF>2.0.CO;2](https://doi.org/10.1175/1520-0469(1988)045<1228:TGOGRF>2.0.CO;2).
- Seo, K.-H., and S.-W. Son, 2012: The global atmospheric circulation response to tropical diabatic heating associated with the Madden–Julian oscillation during northern winter. *J. Atmos. Sci.*, **69**, 79–96, doi:[10.1175/2011JAS3686.1](https://doi.org/10.1175/2011JAS3686.1).
- Sinclair, M. R., 1997: Objective identification of cyclones and their circulation intensity and climatology. *Wea. Forecasting*, **12**, 595–612, doi:[10.1175/1520-0434\(1997\)012<0595:OIOCAT>2.0.CO;2](https://doi.org/10.1175/1520-0434(1997)012<0595:OIOCAT>2.0.CO;2).
- Straus, D. M., E. Swenson, and C. Lappen, 2015: The MJO cycle forcing of the North Atlantic circulation: Intervention experiments with the Community Earth System Model. *J. Atmos. Sci.*, **72**, 660–681, doi:[10.1175/JAS-D-14-0145.1](https://doi.org/10.1175/JAS-D-14-0145.1).
- Taguchi, B., H. Nakamura, M. Nonaka, and S.-P. Xie, 2009: Influences of the Kuroshio/Oyashio Extensions on air–sea heat exchanges and storm-track activity as revealed in regional atmospheric model simulations for the 2003/04 cold season. *J. Climate*, **22**, 6536–6559, doi:[10.1175/2009JCLI2910.1](https://doi.org/10.1175/2009JCLI2910.1).
- Takahashi, C., and R. Shirooka, 2014: Storm track activity over the North Pacific associated with the Madden–Julian Oscillation under ENSO conditions during boreal winter. *J. Geophys. Res. Atmos.*, **119**, 10 663–10 683, doi:[10.1002/2014JD021973](https://doi.org/10.1002/2014JD021973).
- Trenberth, K. E., 1991: Storm tracks in the Southern Hemisphere. *J. Atmos. Sci.*, **48**, 2159–2178, doi:[10.1175/1520-0469\(1991\)048<2159:STITSH>2.0.CO;2](https://doi.org/10.1175/1520-0469(1991)048<2159:STITSH>2.0.CO;2).
- Waliser, D. E., 2006: Intraseasonal variability. *The Asian Monsoon*, B. Wang, Ed., Springer, 203–257.
- Wallace, J. M., and D. Gutzler, 1981: Teleconnection in the geopotential height field during the Northern Hemisphere winter. *Mon. Wea. Rev.*, **109**, 784–812, doi:[10.1175/1520-0493\(1981\)109<0784:TITGHF>2.0.CO;2](https://doi.org/10.1175/1520-0493(1981)109<0784:TITGHF>2.0.CO;2).
- , G.-H. Lim, and M. L. Blackmon, 1988: Relationship between cyclone tracks, anticyclone tracks and baroclinic waveguides. *J. Atmos. Sci.*, **45**, 439–462, doi:[10.1175/1520-0469\(1988\)045<0439:RBCTAT>2.0.CO;2](https://doi.org/10.1175/1520-0469(1988)045<0439:RBCTAT>2.0.CO;2).
- Weickmann, K. M., G. R. Lussky, and J. E. Kutzbach, 1985: Intraseasonal (30–60 day) fluctuations of outgoing longwave radiation and 250 mb streamfunction during northern winter. *Mon. Wea. Rev.*, **113**, 941–961, doi:[10.1175/1520-0493\(1985\)113<0941:IDFOOL>2.0.CO;2](https://doi.org/10.1175/1520-0493(1985)113<0941:IDFOOL>2.0.CO;2).
- Wheeler, M., and H. H. Hendon, 2004: An all-season real-time multivariate MJO index: Development of an index for monitoring and prediction. *Mon. Wea. Rev.*, **132**, 1917–1932, doi:[10.1175/1520-0493\(2004\)132<1917:AARMMI>2.0.CO;2](https://doi.org/10.1175/1520-0493(2004)132<1917:AARMMI>2.0.CO;2).
- Xia, X., and E. K. M. Chang, 2014: Diabatic damping of zonal index variations. *J. Atmos. Sci.*, **71**, 3090–3105, doi:[10.1175/JAS-D-13-0292.1](https://doi.org/10.1175/JAS-D-13-0292.1).
- Zhang, C., 2005: Madden–Julian oscillation. *Rev. Geophys.*, **43**, RG2003, doi:[10.1029/2004RG000158](https://doi.org/10.1029/2004RG000158).